

Angular cuts to reduce the $\tau\bar{\tau}j$ background to the higgsino signal at the LHC

Howard Baer^{1†}, Vernon Barger^{2‡}, Dibyashree Sengupta^{3§} and Xerxes Tata^{4¶}

¹*Homer L. Dodge Department of Physics and Astronomy,
University of Oklahoma, Norman, OK 73019, USA*

²*Department of Physics, University of Wisconsin, Madison, WI 53706 USA*

³*Department of Physics, National Taiwan University, Taipei, Taiwan 10617, R.O.C.*

⁴*Department of Physics and Astronomy, University of Hawaii, Honolulu, HI, USA*

Abstract

We re-examine higgsino pair production in association with a hard QCD jet at the LHC. We focus on $\ell^+\ell^- + \cancel{E}_T + j$ events from the production and subsequent decay, $\tilde{\chi}_2^0 \rightarrow \tilde{\chi}_1^0 \ell^+ \ell^-$, of the heavier neutral higgsino. The novel feature of our analysis is that we propose angular cuts to reduce the irreducible background from $Z(\rightarrow \tau\bar{\tau}) + j$ events more efficiently than the $m_{\tau\tau}^2 < 0$ cut that has been used by the ATLAS and CMS collaborations. Additional cuts, needed to reduce backgrounds from $t\bar{t}$, WWj and $W/Z + \ell\bar{\ell}$ production, are also delineated. We evaluate the reach of LHC14 for 300 and 3000 fb⁻¹ and stress that the dilepton mass distribution would serve to characterize the higgsino signal.

Submitted to the Proceedings of the US Community Study
on the Future of Particle Physics (Snowmass 2021)

[†]Email: baer@ou.edu

[‡]Email: barger@pheno.wisc.edu

[§]Email: dsengupta@phys.ntu.edu.tw

[¶]Email: tata@phys.hawaii.edu

Executive Summary

The ATLAS and CMS collaborations have been searching for light higgsinos with a compressed spectrum – whose existence is, perhaps, the most robust prediction of natural SUSY – via monojet events with an additional soft e^+e^- or $\mu^+\mu^-$ pair, coming mainly from the decay $\chi_2^0 \rightarrow \chi_1^0 \ell \bar{\ell}$. $Z(\rightarrow \tau\bar{\tau}) + j$ production (where both taus decay leptonically) is an important irreducible SM background to the higgsino signal. This background can be considerably reduced by requiring that $m_{\tau\tau}^2 < 0$, where $m_{\tau\tau}^2$ is constructed in the approximation (valid for relativistic taus from Z decays) that the tau decay products are collinear with the parent tau direction. **We have devised angular cuts that reduce the tau pair plus jet background much more efficiently than this di-tau mass cut.**

Our results are exhibited in the Table below for three SUSY benchmark points, BM1, BM2 and BM3 with a higgsino masses around 150, 200 and 300 GeV and $\Delta m \sim 12, 16$ and 4.3 GeV, respectively. Also shown are the important SM backgrounds. We see that while the di-tau mass cut reduces the tau background by about a factor of 4 (row 2), the angle cuts reduce this by a factor of 50 (row 3) with a relatively small loss in signal efficiency. The last line shows the signal and the background after additional cuts necessary to reduce the other backgrounds.

cuts/process	BM1	BM2	BM3	$\tau\bar{\tau}j$	$t\bar{t}$	WWj	$W\ell j$	$Z\ell\ell j$
Basic cuts	1.2	0.19	0.07	94.2	179	35.9	14.7	5.9
Basic+ $m_{\tau\tau}^2 < 0$	0.92	0.13	0.043	23.1	75.6	12.8	7.7	3.2
Basic+angle	0.68	0.12	0.04	1.8	130	22	11.0	4.9
Additional cuts	0.25	0.032	0.017	0.088	0.29	0.39	0.15	0.07

Table: Cross sections (in fb) for signal benchmark points and the various SM backgrounds.

Our projected reach for the signal at the LHC with 300 fb^{-1} and for 3000 fb^{-1} is shown by dashed lines in the figure, and compared with corresponding projections for the HL-LHC obtained by the ATLAS and CMS collaborations.

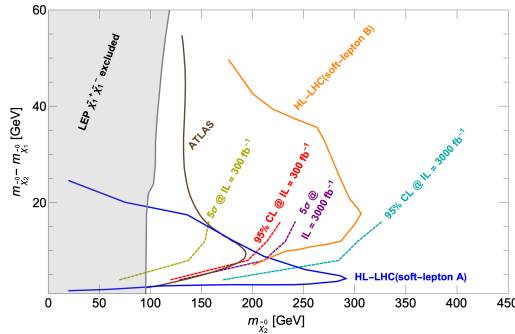


Figure: Our projections for the LHC reach (dashed lines) along with the current 95% CL exclusion (ATLAS) and the projected 95% CL exclusions from two different analyses for the HL-LHC.

1 Introduction

It is generally expected that higgsinos cannot be much heavier than the electroweak scale if weak scale supersymmetry is the new physics that stabilizes the Higgs sector [1]. The precise upper limit on the higgsino mass depends on the degree of fine-tuning that is considered acceptable: for no worse than a part in thirty electro-weak fine-tuning ($\Delta_{\text{EW}} < 30$) [2], higgsinos are expected to be lighter than ~ 350 GeV, while all other super-partners could be in the multi-TeV range [2,3]. For this reason, the search for light higgsinos has become an important part of the experimental SUSY program at the LHC [4,5].

In the generic situation of natural SUSY models where electroweak gauginos are much heavier than the higgsinos (gauginos with multi-TeV masses do not destabilize the Higgs vacuum-expectation-value) the mass splitting between the two lightest neutral higgsinos is very small— $\sim 4\text{--}25$ GeV—so that the visible products of higgsino decays to the (higgsino-like) LSP¹ are correspondingly soft. As a result, although higgsino pair production cross sections at LHC14 are substantial ($\sim 100 - 1000$ fb for higgsino masses in the 120–350 GeV range), the visible decay products from higgsino pair production may be hidden under enormous backgrounds from Standard Model (SM) processes [6]. Because the visible decay products of the higgsinos are— for practical purposes— invisible, this led to the suggestion that it might be possible to search for higgsino pairs produced in association with a hard object X , where X is a mono-jet [7], mono-photon [8], mono-gauge boson [9] or mono-Higgs boson [10]. While it is possible to gain a statistical significance of the signal exceeding 5σ by requiring a hard enough cut on the mono-jet, the signal to background ratio is at the $\sim 1\%$ level, so that this strategy is viable only if the backgrounds can be controlled to percent level or below precision.

An alternative strategy is to detect the *soft leptons* produced via higgsino decays in higgsino pair events triggered by a hard monojet (or the \cancel{E}_T) to further reduce the SM background [11–14]. Dileptons from $\tilde{\chi}_2^0$ decays would necessarily be of opposite sign (OS) and the same flavour (SF), and further, their invariant mass is kinematically bounded above by $\Delta m \equiv m_{\tilde{\chi}_2^0} - m_{\tilde{\chi}_1^0}$. The higgsino mono-jet plus soft dilepton signal has been studied by several groups, and has been used by both the ATLAS [4] and CMS [5] collaborations for their searches for higgsinos with a compressed spectrum. The main purpose of this note is to point out an analysis strategy involving *angular cuts* that is more effective than the currently used method that uses the di-tau invariant mass to beat down the important SM background to the higgsino signal arising from tau pair production in association with a hard jet (the leptons come from the decays of the taus). We also delineate other cuts that reduce the other backgrounds, and map out the reach of the HL-LHC in the $m_{\tilde{\chi}_2^0}$ vs. Δm mass plane. This Snowmass 2021 contribution summarizes and streamlines the results of Ref. [15] with an emphasis on the angular cuts to reduce the important irreducible background from $Z \rightarrow \tau\bar{\tau}$ events.

¹We assume conservation of R -parity and also note that the lightest, thermally produced higgsino comprises only a portion of the observed relic cold dark matter abundance.

2 Higgsino Signal and SM background processes

We focus on the signal from higgsino pair production in association with a QCD jet at the LHC: $pp \rightarrow \tilde{\chi}_1^+ \tilde{\chi}_1^-, \tilde{\chi}_1^0 \tilde{\chi}_2^0, \tilde{\chi}_1^\pm \tilde{\chi}_2^0 + j$, where $\tilde{\chi}_1^\pm \rightarrow \ell \nu \tilde{\chi}_1^0$ and $\tilde{\chi}_2^0 \rightarrow \ell \bar{\ell} \tilde{\chi}_1^0$ ($\ell = e, \mu$). Requiring a hard jet boosts the lepton daughters of the higgsino in addition to providing a trigger for the events. We evaluate SM backgrounds to the monojet plus OS/SF dilepton higgsino signal from:

- $\tau \bar{\tau} j$ production,
- $t \bar{t}$ production,
- WWj production,
- $W \ell \bar{\ell} j$ production, and
- $Z \ell \bar{\ell} j$ production

in the SM.

For our calculations, we use MADGRAPH 2.5.5 [16] interfaced to PYTHIA v8 [17] via the default MadGraph/PYTHIA interface with default parameters for showering and hadronization to generate pp collision events with $\sqrt{s} = 14$ TeV. Detector simulation is performed by DELPHES using the default Delphes 3.4.2 [18] “ATLAS” parameter card. We adopt the anti- k_T jet algorithm [19] with $R = 0.6$, the default value in the ATLAS Delphes card, to form jets. Jet finding in Delphes is implemented via FASTJET [20]. We consider only jets with transverse energy satisfying $E_T(jet) > 40$ GeV and pseudorapidity satisfying $|\eta(jet)| < 3.0$ in our analysis. Jet finding in Delphes is implemented via FASTJET [20]. We consider only jets with transverse energy satisfying $E_T(jet) > 40$ GeV and pseudorapidity satisfying $|\eta(jet)| < 3.0$ in our analysis. We implement the default Delphes b -jet tagger and implement a b -tag efficiency of 85% [21]. We identify leptons with $E_T > 5$ GeV and within $|\eta(\ell)| < 2.5$. We label them as *isolated leptons* if the sum of the transverse energy of all other objects (tracks, calorimeter towers, etc.) within $\Delta R = 0.5$ of the lepton candidate is less than 10% of the lepton E_T .

In order to assess the level of the SUSY signal relative to the SM backgrounds, we have selected three benchmark points with varying higgsino masses and varying mass gaps between the heavier higgsinos and the LSP: the higgsino production rate obviously depends on the higgsino mass, and the lepton detection efficiency is very sensitive to the higgsino mass gap, Δm . We use the computer code Isajet 7.88 [22] to generate sparticle masses. The resulting SUSY Les Houches Accord (SLHA) files are then used as inputs to Madgraph/Pythia/Delphes for event generation.

The first two benchmark points, BM1 and BM2, are obtained from the two-extra-parameter non-universal Higgs model (NUHM2) with parameters $m_0, m_{1/2}, A_0, \tan \beta, \mu, m_A$ and have higgsino masses around 150 GeV and 300 GeV, respectively, and corresponding mass gaps $\Delta m = 12$ GeV and 16 GeV. Although not critical for a discussion of the phenomenology of the signal, we note that both these benchmark points satisfy our naturalness criterion, $\Delta_{EW} < 30$. The third point, labeled as BM3 (GMM') has higgsino masses around 200 GeV and a small $\Delta m \simeq 4.3$ GeV. Since NUHM2 models with $\Delta_{EW} < 30$ necessarily have $\Delta m \gtrsim 10$ GeV, we have used the natural generalized mirage mediation model [23], where μ is an input, to generate a benchmark point with this small mass gap; this, of course, makes the signal search

a challenge even though the higgsinos are not particularly heavy. The input parameters and SUSY spectra from the benchmark points are listed in Table 1, along with some low energy and dark-matter-related observables along with the degree of electroweak fine-tuning, which we view as a conservative measure of naturalness.

3 Higgsino Signal Analysis

For the SUSY signal from higgsinos, we generate events from the reactions $pp \rightarrow \tilde{\chi}_1^\pm \tilde{\chi}_2^0 j$, $\tilde{\chi}_1^0 \tilde{\chi}_2^0 j$ and $\tilde{\chi}_1^\pm \tilde{\chi}_1^\mp j$, where $\tilde{\chi}_2^0 \rightarrow \tilde{\chi}_1^0 \ell^+ \ell^-$ and $\tilde{\chi}_1^\pm \rightarrow \ell \nu \tilde{\chi}_1^0$. The dilepton plus jet signal together with the cross sections from the various backgrounds listed in Sec. 2, after a series of cuts described below, is shown in Table 2. The first entry labeled *BC* (for *before cuts*) actually has parton level cuts implemented at the Madgraph level. These cuts serve to regularize subprocesses that are otherwise divergent. Also, for the backgrounds with a hard QCD ISR (labeled as *j* in the table header), we require $p_T(j) > 80$ GeV to efficiently generate events with a hard jet. For the backgrounds including $\gamma^*, Z^* \rightarrow \ell \bar{\ell}$ ($\ell = e$ or μ), we require $m(\ell \bar{\ell}) > 1$ GeV. We also require $p_T(\ell) > 1$ GeV and $\Delta R(\ell \bar{\ell}) > 0.01$, again at the parton level. The W daughters of top quarks in $t\bar{t}$ events are forced to decay leptonically (into e , μ or τ), but not so the W -bosons in first entry of the WWj column. These parton events are then fed into PYTHIA and analysed using the DELPHES detector simulation. The leading order cross sections (in fb), for both the signal as well as for the backgrounds, are listed in row 1, labelled *BC*. At this stage, the signal is dwarfed by SM backgrounds.

To select out signal events, we require:

- two opposite sign, same flavour (OS/SF) isolated leptons with $p_T(\ell) > 5$ GeV, $|\eta(\ell)| < 2.5$,
- there be at least one jet in the event, *i.e.*, $n_j \geq 1$ with $p_T(j_1) > 100$ GeV for identified calorimeter jets,
- $\Delta R(\ell \bar{\ell}) > 0.05$ (for $\ell = e$ or μ),
- $E_T > 100$ GeV, and
- a veto of tagged b -jets, $n(b\text{-jet})=0$.

The cross sections after this set of cuts, labeled as **C1** are shown in the next row of Table 2. At this stage, the leading irreducible physics background from $\tau \bar{\tau} j$ events is two orders of magnitude larger than the signal, while the background from top pair production (which nominally contains two untagged b -jets) is a factor of two larger than this.

3.1 Reducing the di-tau plus jet background

3.1.1 $m_{\tau\tau}^2$ cut

After **C1** cuts, the decay $Z \rightarrow \tau \bar{\tau}$ of an on-shell high p_T Z boson recoiling against a hard QCD jet is the leading source of the $\tau \bar{\tau} j$ events. This means that this background can be greatly reduced if it would be possible to reconstruct the di-tau invariant mass *despite the presence of*

parameter	<i>BM1</i>	<i>BM2</i>	<i>BM3 (GMM')</i>
m_0	5000	5000	–
$m_{1/2}$	1001	1000	–
A_0	-8000	-8000	–
$\tan \beta$	10	10	10
$m_{3/2}$	–	–	75000
α	–	–	4
c_m	–	–	6.9
c_{m3}	–	–	6.9
a_3	–	–	5.1
μ	150	300	200
m_A	2000	2000	2000
$m_{\tilde{g}}$	2425.4	2422.6	2837.3
$m_{\tilde{u}_L}$	5295.9	5295.1	5244.6
$m_{\tilde{u}_R}$	5427.8	5426.5	5378.0
$m_{\tilde{e}_R}$	4823.7	4824.5	4813.2
$m_{\tilde{t}_1}$	1571.7	1578.4	1386.9
$m_{\tilde{t}_2}$	3772.0	3773.0	3716.7
$m_{\tilde{b}_1}$	3806.7	3807.6	3757.8
$m_{\tilde{b}_2}$	5161.2	5160.2	5107.7
$m_{\tilde{\tau}_1}$	4746.8	4747.5	4729.8
$m_{\tilde{\tau}_2}$	5088.6	5088.2	5075.7
$m_{\tilde{\nu}_\tau}$	5095.4	5095.0	5084.8
$m_{\tilde{\chi}_2^\pm}$	-857.1	-857.6	-1801.9
$m_{\tilde{\chi}_1^\pm}$	-156.6	-311.6	-211.1
$m_{\tilde{\chi}_4^0}$	-869.0	-869.8	-1809.3
$m_{\tilde{\chi}_3^0}$	-451.3	-454.7	-1554.4
$m_{\tilde{\chi}_2^0}$	157.6	310.1	207.0
$m_{\tilde{\chi}_1^0}$	-145.4	-293.7	-202.7
m_h	124.5	124.6	125.4
$\Omega_{\tilde{\chi}_1^0}^{std} h^2$	0.007	0.023	0.009
$BF(b \rightarrow s\gamma) \times 10^4$	3.1	3.1	3.1
$BF(B_s \rightarrow \mu^+ \mu^-) \times 10^9$	3.8	3.8	3.8
Δ_{EW}	13.9	21.7	26.0

Table 1: Input parameters and sparticle masses in GeV units for the two NUHM2 model benchmark points (BM1 and BM2) and one natural mirage mediation SUSY benchmark point (BM3 (GMM')) introduced in the text. We take $m_t = 173.2$ GeV. The input parameters for the natural(generalized) mirage mediation model such as α and c_m have been calculated from m_0^{MM} and $m_{1/2}^{MM}$ which are taken equal to the corresponding NUHM2 model values of m_0 and $m_{1/2}$, respectively. The c_m and c_{m3} have been taken equal to each other so that masses of first/second and third generation sfermions are equal at the GUT scale so as to also match the NUHM2 models in the second and third columns of the table.

cuts/process	$BM1$	$BM2$	$BM3(GMM')$	$\tau\bar{\tau}j$	$t\bar{t}$	WWj	$W\ell\ell j$	$Z\ell\ell j$
BC	83.1	9.3	31.3	43800.0	41400	9860	1150.0	311
$C1$	1.2	0.19	0.07	94.2	179	35.9	14.7	5.9
$C1 + m_{\tau\tau}^2 < 0$	0.92	0.13	0.043	23.1	75.6	12.8	7.7	3.2
$C1 + angle$	0.68	0.12	0.04	1.8	130	22	11.0	4.9
$C2$	0.29	0.049	0.019	0.088	0.99	0.49	0.18	0.14
$C3$	0.25	0.032	0.017	0.088	0.29	0.39	0.15	0.07

Table 2: Cross sections (in fb) for signal benchmark points and the various SM backgrounds listed in the text after various cuts. The row labelled BC denotes parton level cross sections after the requirement $p_T(j) > 80$ GeV, along with minimal cuts implemented to regulate divergences, and also includes the leptonic branching fractions for decays of both the top quarks in the $t\bar{t}$ column. The remaining rows list the cross sections after a series of analysis cuts detailed in the text.

the neutrinos that are present when the taus decay leptonically. This is possible because the taus from Z -boson decays are typically very relativistic. In the approximation that the leptons and neutrinos from the decay of a relativistic tau are all exactly collimated along the parent tau direction, we can write the momentum carried off by the two neutrinos from the decay $\tau_1 \rightarrow \ell_1 \bar{\nu}_{\ell_1} \nu_{\tau_1}$ of the first tau as $\xi_1 \vec{p}(\ell_1)$ and, similarly, as $\xi_2 \vec{p}(\ell_2)$ for the second tau. Momentum conservation in the plane transverse to the beams then requires that

$$-\sum_{jets} \vec{p}_T(j) = (1 + \xi_1) \vec{p}_T(\ell_1) + (1 + \xi_2) \vec{p}_T(\ell_2). \quad (1)$$

These two equations can be solved for ξ_1 and ξ_2 given that $\vec{p}_T(j)$ and $\vec{p}_T(\ell_{1,2})$ are all measured, and used to evaluate the momenta of the individual taus. This then allows us to evaluate the invariant mass squared of the di-tau system which (within the collinear approximation for tau decays) is given by,

$$m_{\tau\tau}^2 = (1 + \xi_1)(1 + \xi_2)m_{\ell\ell}^2. \quad (2)$$

We show the distribution of $m_{\tau\tau}^2$ constructed using Eq. (2) for both signal events as well as for the various backgrounds in Fig. 1 after the cut set **C1** and also requiring $n_j = 1$ to further reduce the top background. As expected, this peaks sharply around m_Z^2 for the $\tau\bar{\tau}j$ events (red histogram). In contrast, for signal and other SM background sources, where the isolated lepton and \vec{E}_T directions are uncorrelated, the $m_{\tau\tau}^2$ distributions are very broad and peak at even negative values of $m_{\tau\tau}^2$. The $m_{\tau\tau}^2$ variable provides a very good discriminator between $\tau\bar{\tau}j$ background and signal. The cut $m_{\tau\tau}^2 < 0$ [13] has, in fact, been used in ATLAS [4] and CMS [5] for their analyses. We see from the third row of Table 2 that the $\tau\bar{\tau}j$ background is reduced by a factor ~ 4 while the signal is reduced by 25-40%. The efficiency with which the di-tau background is reduced is limited because the tail of the $\tau\bar{\tau}j$ background extends out to negative values of $m_{\tau\tau}^2$; this happens because of tau pair production from virtual photons, the breakdown of the collinear approximation for asymmetric Z decays and finally hadronic energy mismeasurements which skew the direction of both $\vec{p}_T(j)$ and of \vec{E}_T . In Sec.3.1.2, we describe angle cuts which can reduce the di-tau background very efficiently with only moderate loss of

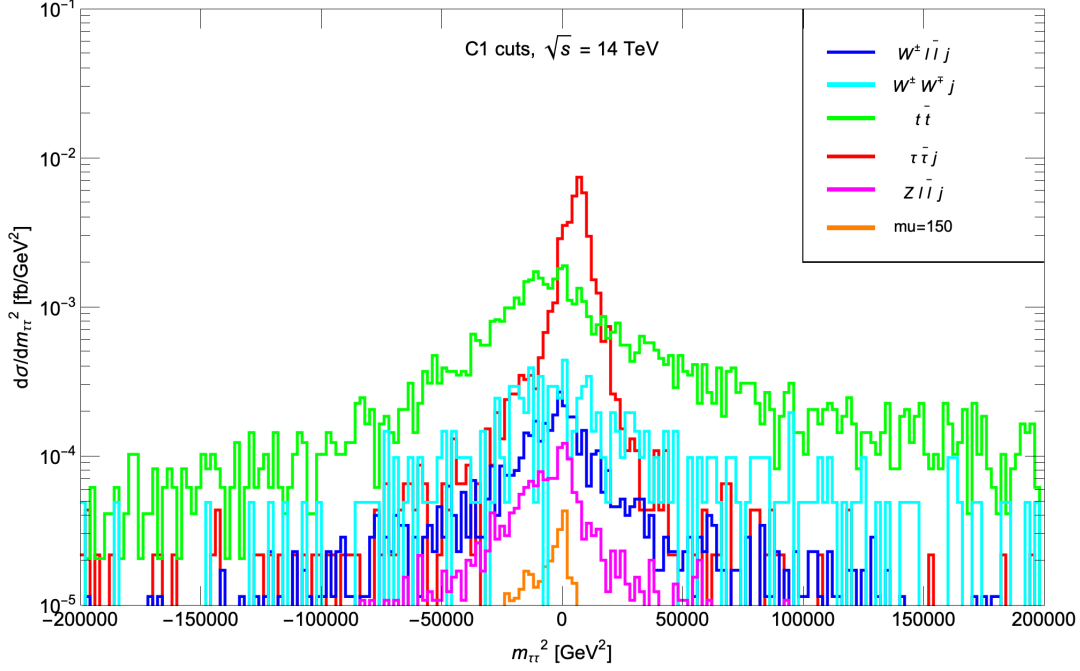


Figure 1: Distribution in $m_{\tau\tau}^2$ for the three SUSY BM models with $\mu = 150, 200$ and 300 GeV introduced in the text, along with SM backgrounds after $C1$ cuts augmented by $n_j = 1$.

the higgsino signal, and suggest that these replace the $m_{\tau\tau}^2 < 0$ cut that has been used by ATLAS and CMS for their compressed higgsino search.

3.1.2 Angle cuts

In the transverse plane, the di-tau pair must recoil against the hard QCD radiation with the transverse plane opening angle between the taus significantly smaller than π . The central idea behind our proposal is that, in the transverse plane, the \vec{E}_T vector *must lie between the directions of the two taus*. For relativistic taus, the tau direction is, of course, essentially the same as the *observable* direction of its charged lepton daughter as illustrated in Fig. 2. We require the azimuthal angles ϕ_ℓ and $\phi_{\bar{\ell}}$ for each lepton to lie between 0 and 2π , and define $\phi_{max} = \max(\phi_\ell, \phi_{\bar{\ell}})$ and $\phi_{min} = \min(\phi_\ell, \phi_{\bar{\ell}})$. Then for \vec{E}_T to lie in between the tau daughter lepton directions we must have,²

$$\phi_{min} < \phi_{E_T} < \phi_{max}.$$

Notice that, by definition, $\phi_{max} - \phi_{min} < \pi$, and for a boosted tau pair, often significantly smaller than π .

To characterize the $Z(\rightarrow \tau\bar{\tau}) + j$ background, we show in Fig. 3 a scatter plot of these events in the $\phi_1 \equiv \phi_{max} - \phi_{E_T}$ vs. $\phi_2 \equiv \phi_{E_T} - \phi_{min}$ plane. If the collinear approximation for

²This works as long as $|\phi_\ell - \phi_{\bar{\ell}}| < \pi$. If $|\phi_\ell - \phi_{\bar{\ell}}| > \pi$, define $\phi'_\ell = \phi_\ell + \pi$, $\phi'_{\bar{\ell}} = \phi_{\bar{\ell}} + \pi$ and $\phi'_{E_T} = \phi_{E_T} + \pi$, (all modulo 2π) along with $\phi_{max} = \max(\phi'_\ell, \phi'_{\bar{\ell}})$, and likewise, $\phi_{min} = \min(\phi'_\ell, \phi'_{\bar{\ell}})$, and then require, $\phi_{min} < \phi_{E_T} < \phi_{max}$.

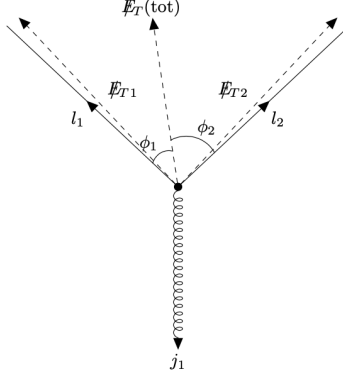


Figure 2: Sketch of a ditau background event to the di-lepton plus jet plus \cancel{E}_T signature in the transverse plane of the event. Here ℓ_1 and \cancel{E}_{T1} denote the transverse momentum of the lepton and of the vector sum of the neutrinos from the decay of the first tau, and likewise ℓ_2 and \cancel{E}_{T2} . $\cancel{E}_T(\text{tot})$ is the resultant \cancel{E}_T in the event. Notice that because the taus are expected to be relativistic, ℓ_i and \cancel{E}_{Ti} vectors are nearly collimated along the direction of the i^{th} tau ($i = 1, 2$).

tau decays holds, we would expect that the $\tau\bar{\tau}j$ background selectively populates the top right quadrant with $\phi_1 > 0$ and $\phi_2 > 0$ with $\phi_1 + \phi_2 = \phi_{\text{max}} - \phi_{\text{min}} < \pi$, and significantly smaller than π when the tau pair emerges with a small opening angle in the transverse plane. We see from the figure that there is a small, but significant, “spill-over” into the region where ϕ_1 or ϕ_2 assumes small negative values; *i.e.* where $\vec{\cancel{E}}_T$ lies just outside the cone formed by $\vec{\ell}_1$ and $\vec{\ell}_2$. This spill-over arises from asymmetric decays of the Z where one of the taus (the one emitted backwards from the Z direction) is not as relativistic so that the collinear approximation works rather poorly, or because hadronic energy mismeasurements skew the direction of $\vec{\cancel{E}}_T$. Indeed we see from the top frame of Fig. 3 that the $\tau\bar{\tau}j$ background mostly populates the triangle in the top-right quadrant of the ϕ_1 vs. ϕ_2 plane, and $\phi_1 + \phi_2 < f\pi$ where the fraction $0 < f < 1$, with a spill-over into the strips where one of $\phi_{1,2}$ is slightly negative. For signal events and for the other backgrounds, ϕ_{E_T} will be uncorrelated with ϕ_{min} and ϕ_{max} , and so their scatter plots will extend to the other quadrants. This is illustrated for the $t\bar{t}$ background in the middle frame of Fig. 3 and for signal point BM1 in bottom frame. In these cases, we indeed see a wide spread in ϕ_1 and ϕ_2 between $\pm 2\pi$.

To efficiently veto the $\tau\bar{\tau}j$ background, we examined nine cases of angular cuts [15]. Specifically, we allowed $f = 1, 2/3$ and $1/2$ to optimize the effect of the boost of the di-tau on the transverse plane opening angle, and also allowed for the width of the spill-over strip (to negative values of ϕ_1 or ϕ_2) equal to 0, $\pm\pi/20$ and $\pm\pi/10$. We found that $S/\sqrt{BG(\tau\bar{\tau}j)}$ was optimized for LHC14 with 3000 fb^{-1} when we,

$$\text{veto the triangle } \phi_1, \phi_2 > 0 \text{ with } \phi_1 + \phi_2 < \pi/2, \quad (3)$$

along with an additional veto to further reduce background from the spill-over of $\vec{\cancel{E}}_T$ outside of the cone defined by the charged leptons:

$$\text{strip cuts : veto } |\phi_{1,2}| < \pi/10, \text{ and veto } \phi_{1,2} \text{ in the two corner strips.} \quad (4)$$

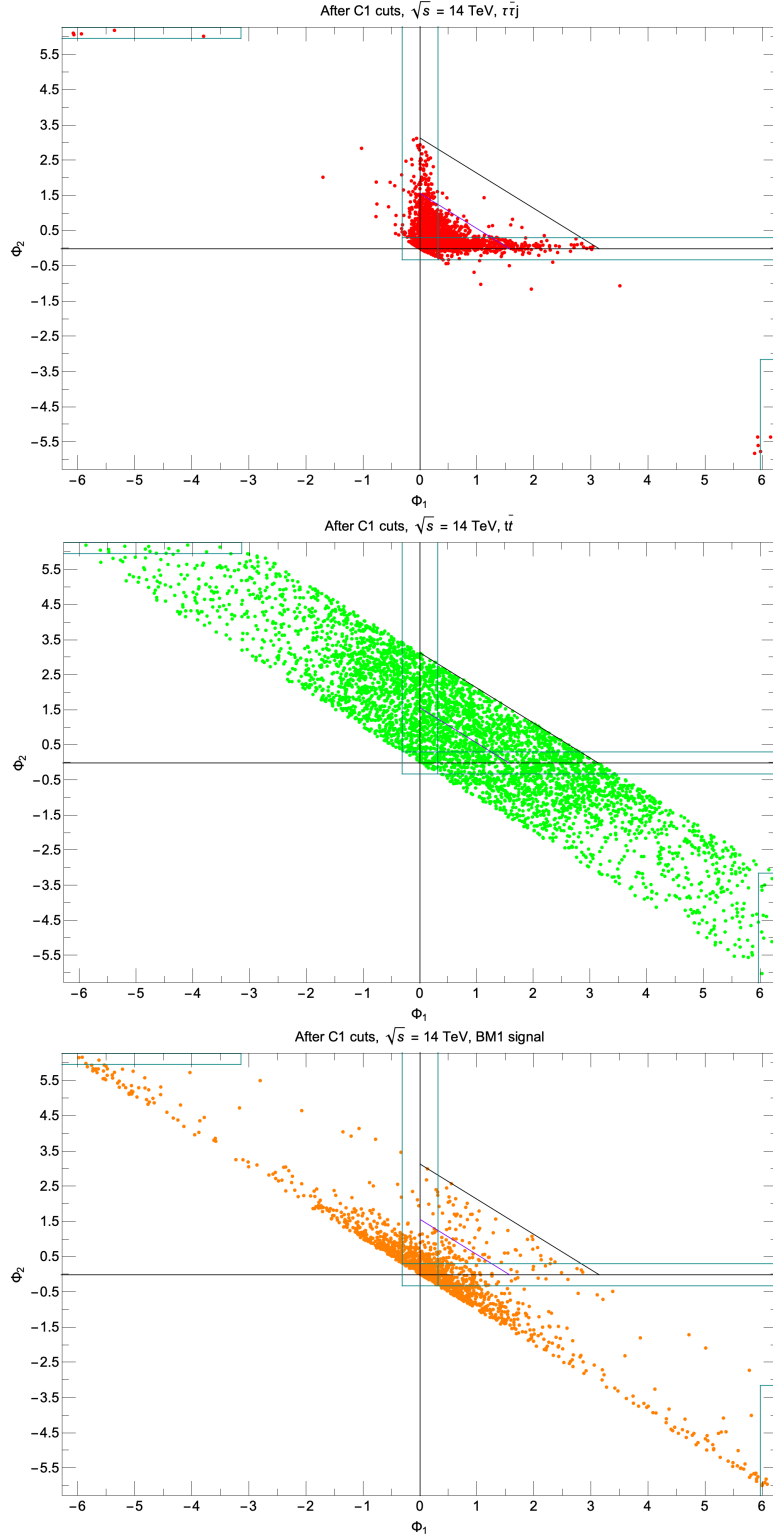


Figure 3: Scatter plots in the ϕ_1 vs. ϕ_2 plane for $\tau\tau j$ and $t\bar{t}$ backgrounds and for the signal point BM1 after $C1$ cuts, requiring also that $n_j = 1$. Also shown are the lines where $\phi_1 + \phi_2 < \pi/2, \pi$ along with the strip cuts in Eq. (4). In the strips in the top left and bottom right of each frame and along the positive ϕ_1 and ϕ_2 axes, $E_T^{\vec{\ell}}$ is close to the boundary of the lepton cone.

In the horizontal (vertical) strip in the upper left (lower right) quadrant of each frame of Fig. 3, ϕ_2 (ϕ_1) is within $\pi/10$ of 2π which, of course, is the same $-\pi/10 < \phi_{1,2} < 0$ (modulo 2π), and hence just outside the lepton cone.

We list signal and background rates after **C1** cuts together with the cuts (3) and (4) – collectively referred to as *angle cuts* from this point on – in row 4 of Table 2. In this case, we find that $\tau\bar{\tau}j$ background is reduced from cut set **C1** by a factor ~ 52 (compared to a factor ~ 4 for the $m_{\tau\tau}^2 < 0$ cut) whilst signal efficiency for the point BM1 is almost 60% (compared to $\sim 75\%$ for the $m_{\tau\tau}^2 < 0$ cut). We also see that signal efficiency for the other two benchmark points is nearly the same for the angular and for the $m_{\tau\tau}^2 < 0$ cuts. We regard the angular cuts as a significantly improved method for almost completely removing the irreducible $\tau\bar{\tau}j$ background. The other SM backgrounds are not as efficiently reduced by the angular cut as by the $m_{\tau\tau}^2 < 0$ cut, and need other cuts to reduce them to manageable levels.

3.2 Further cuts to remove top and W -pair backgrounds

We have just seen that while the angle cuts greatly reduce the irreducible $\tau\bar{\tau}j$ background, SM backgrounds from $t\bar{t}$ and WWj events (followed by leptonic decays of the top and W -bosons) and also from $W/Z\ell\bar{\ell} + j$ production still completely dwarf the signal. Since the top pair background typically has a higher jet multiplicity, requiring $n_j = 1$ increases the signal-to-background ratio (as already mentioned earlier). The hard jet and \cancel{E}_T distributions are both backed up against their cut value, and given the already small signal cross section, it is not helpful to require a harder cut on these variables.

In contrast, the transverse momenta of the leptons from on-shell top and W decays then have broader distributions than the signal leptons. We found that requiring upper limits on $|p_T(\ell_2)|$ and $H_T(\ell\bar{\ell}) \equiv |p_T(\ell_1)| + |p_T(\ell_2)|$ indeed enhances the signal over the background [15]. The transverse momenta of leptons and neutrinos from W and top decays have comparable magnitudes; in contrast the momentum scale for signal leptons is set by Δm while that for signal \cancel{E}_T is set by the higgsino mass. As a result, the ratio $\cancel{E}_T/H_T(\ell\bar{\ell})$ is expected to be considerably harder for the higgsino signal than for the SM background as first noted by the ATLAS collaboration [24]. Finally, we note that the dilepton mass distribution for leptons from $\tilde{\chi}_2^0 \rightarrow \tilde{\chi}_1^0 \ell\bar{\ell}$ decays is kinematically bounded by $m(\ell\bar{\ell}) < m_{\tilde{\chi}_2^0} - m_{\tilde{\chi}_1^0} \lesssim 20 - 25$ GeV for the compressed higgsino search, and further, that the invariant mass of dileptons from $\tilde{\chi}_1^+ \tilde{\chi}_1^-$ production events will also tend to be smaller than for background events, simply because leptons from the chargino decays are soft. Again, we refer the interested reader to Ref. [15] where these distributions and others are explicitly shown.

These considerations lead us to include the analysis cut set **C2** to enhance the higgsino signal over the top and WWj backgrounds that dominate after the angle cuts:

- the cut set **C1** together with the angle cuts,
- $n(jets) = 1$,
- $p_T(\ell_2) : 5 - 15$ GeV,
- $H_T(\ell\bar{\ell}) < 60$ GeV

- $\cancel{E}_T/H_T(\ell\bar{\ell}) > 4$, and
- $m(\ell\bar{\ell}) < 50$ GeV.

We have checked that the requirement $m(\ell\bar{\ell}) < 50$ GeV, efficiently reduces much of the background while retaining most of the higgsino signal.

We see from the penultimate row of Table 2 that after **C2** cuts, the leading $t\bar{t}$ background has dropped by a factor ~ 130 , and the total SM background has dropped to $\sim 1.1\%$, while the signal is retained with an efficiency of 40-60%. At this point, the total background is just below 2 fb. Clearly, the signal cross section is small, and the large integrated luminosities expected at the HL-LHC will be necessary for the detection of the signal if the higgsino mass is close to its naturalness bound of 300-350 GeV, or if the higgsino spectrum is maximally compressed to the 4 – 5 GeV level, consistent with electroweak naturalness.

To further enhance the signal relative to (particularly the top) background, we note that for the signal, where the SUSY particles recoil strongly against the ISR jet, we expect nearly back-to-back $\vec{p}_T(jet)$ and $\vec{\cancel{E}}_T$ vectors. This correlation is expected to be somewhat weaker from $t\bar{t}$ background events and also for $W\ell\bar{\ell}j$ events because these intrinsically contain additional activity from decay products that do not form jets or identified leptons. The dilepton-plus- \cancel{E}_T cluster transverse mass $m_{cT}(\ell\bar{\ell}, \cancel{E}_T)$ and the relative values of $E_T(jet)$ and \cancel{E}_T (which tend to be more balanced for the signal than for the backgrounds) serve to give added distinction between the signal and backgrounds and provide additional discriminators. These considerations led us to impose the additional cut set **C3** that includes:

- all **C2** cuts,
- $\Delta\phi(j_1, \cancel{E}_T) > 2.0$
- $m_{cT}(\ell\bar{\ell}, \cancel{E}_T) < 100$ GeV
- $p_T(j_1)/\cancel{E}_T < 1.5$
- $|p_T(j_1) - \cancel{E}_T| < 100$ GeV.

We show the OS/SF dilepton invariant mass after these **C3** cuts in Fig. 4. The total background, shown in gray, is essentially flat, whereas signal-plus-background is shown by the colored histogram, and correspond to *a*) BM1 with $\Delta m = 12$ GeV, *b*) BM2 with $\Delta m = 16$ GeV and *c*) BM3 with $\Delta m = 4.3$ GeV. The idea here is to look for systematic deviations from SM background predictions in the lowest $m(\ell\bar{\ell})$ bins. Those bins with a notable excess could determine the kinematic limit $m(\ell\bar{\ell}) < m_{\tilde{\chi}_2^0} - m_{\tilde{\chi}_1^0}$. By taking only the bins with a notable excess, *i.e.* $m(\ell\bar{\ell}) < m_{\tilde{\chi}_2^0} - m_{\tilde{\chi}_1^0}$, then it is possible to compute the cut-and-count excess above expected background to determine a discovery limit or exclusion bound. The *shape* of the distribution of the excess below the $\tilde{\chi}_2^0 \rightarrow \tilde{\chi}_1^0 \ell\bar{\ell}$ end point depends on the *relative sign* of the lighter neutralino eigenvalues (these have opposite signs for higgsinos) and so could serve to check the consistency of higgsinos as the origin of the signal [25]. Of the three cases shown, this would be possible at the HL-LHC only for the point BM1, since the tiny signal to background ratio precludes the possibility of determining the signal shape in the other two cases. It may be worthwhile to examine whether sophisticated machine learning methods could lead to a better

signal and background discrimination that allows us to obtain the neutral higgsino mass gap and also the signal shape, particularly for the two difficult cases in Fig. 4

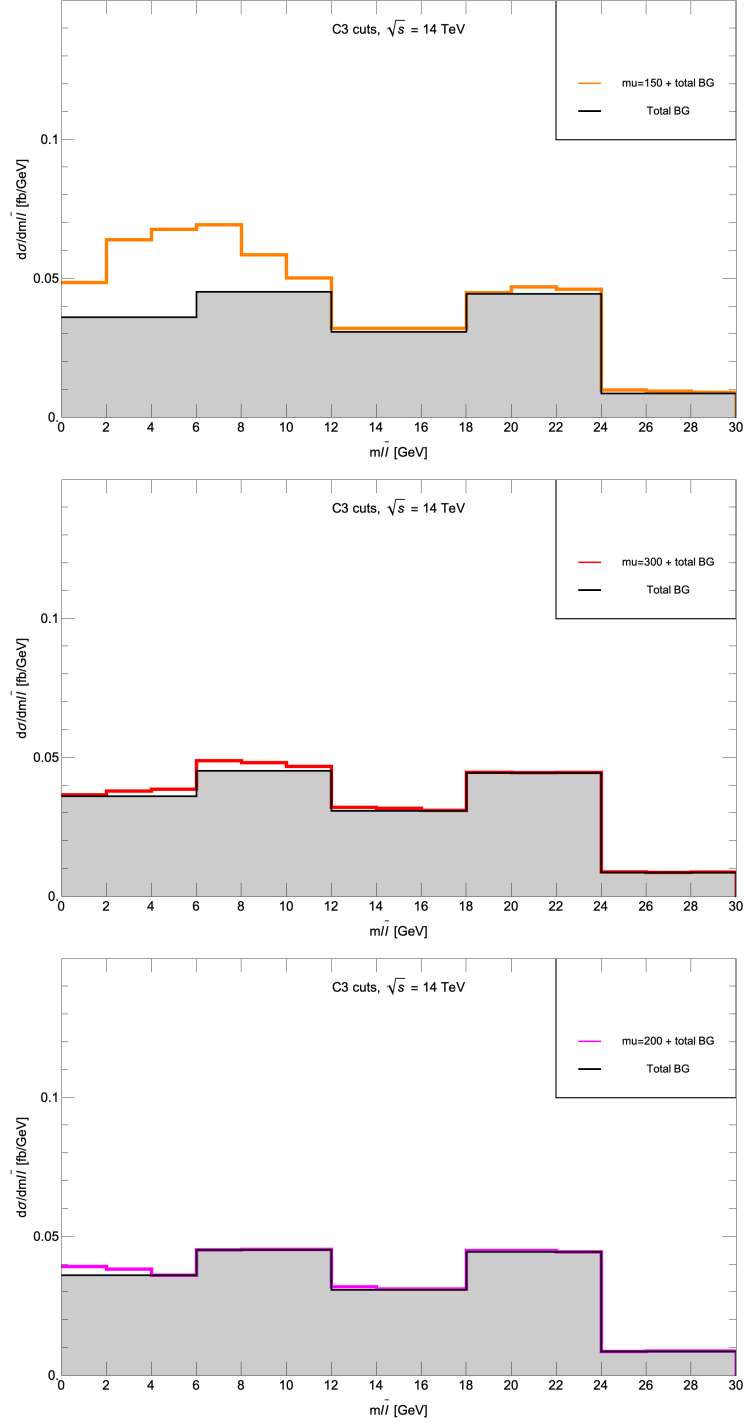


Figure 4: Distribution of $m(\ell^+\ell^-)$ for the three SUSY BM models with $\mu = 150$, 300 and 200 GeV, and for the SM backgrounds after $C3$ cuts.

4 LHC reach for higgsinos with 300-3000 fb⁻¹

The distributions in Fig. 4 suggest that our final analysis cut set **C4** include,

- **C3** cuts, along with
- $m(\ell\bar{\ell}) < m_{\tilde{\chi}_2^0} - m_{\tilde{\chi}_1^0}$.

The location of the mass gap is clearly visible for BM1, but is obscured by the background for the other two cases. To implement the last $m(\ell\bar{\ell})$ cut, we suggest examining the cross section with $m_{\ell\ell} < m_{\ell\ell}^{\text{cut}}$ for varying the value of $m_{\ell\ell}^{\text{cut}}$ and looking for a rise in the event rate where events from $\tilde{\chi}_2^0 \rightarrow \tilde{\chi}_1^0 \ell\bar{\ell}$ would be expected to accumulate. We recognize that with the cut-and-count technique this may not be possible for the difficult cases BM2 and BM3, but in the following, we will optimistically assume that once we have the data, the region where the higgsino signal is beginning to accumulate will be self-evident.

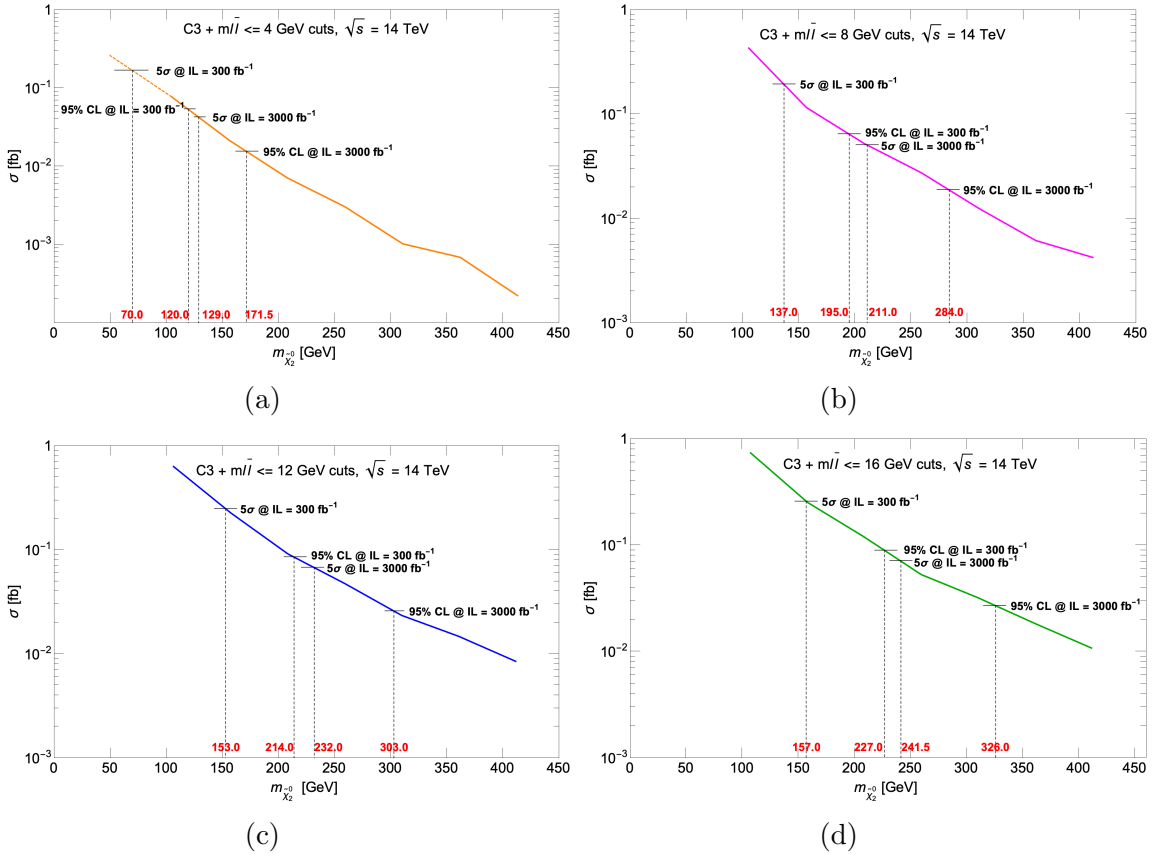


Figure 5: The projected 5σ reach and 95% CL exclusion of the HL-LHC with 3000 fb⁻¹ in μ for four different NUHM2 model lines with a) $\Delta m = 4$ GeV, b) $\Delta m = 8$ GeV, c) $\Delta m = 12$ GeV and d) $\Delta m = 16$ GeV after $C3 + m(\ell\bar{\ell}) < m_{\tilde{\chi}_2^0} - m_{\tilde{\chi}_1^0}$ cuts.

Using these **C4** cuts, then we computed the signal cross section for four model lines in the NUHM2 model for values of μ : 100 – 400 GeV and with $m_{1/2}$ values adjusted such that the

$m_{\tilde{\chi}_2^0} - m_{\tilde{\chi}_1^0}$ mass gap is fixed at 4, 8, 12 and 16 GeV. While μ and $m_{1/2}$ are variable, the values of $m_0 = 5$ TeV, $A_0 = -1.6m_0$, $\tan\beta = 10$ and $m_A = 2$ TeV are fixed for all four model lines. In Fig. 5, we show the signal cross section after **C4** cuts, along with the 5σ reach and the 95% CL exclusion for LHC14 with 300 and 3000 fb^{-1} . We see from Fig. 5 that the HL-LHC typically increases the higgsino reach by about 70-100 GeV (50-60 GeV for the lowest values of $\Delta m = 4$ GeV) as compared to the reach that can be obtained with an integrated luminosity of 300 fb^{-1} .

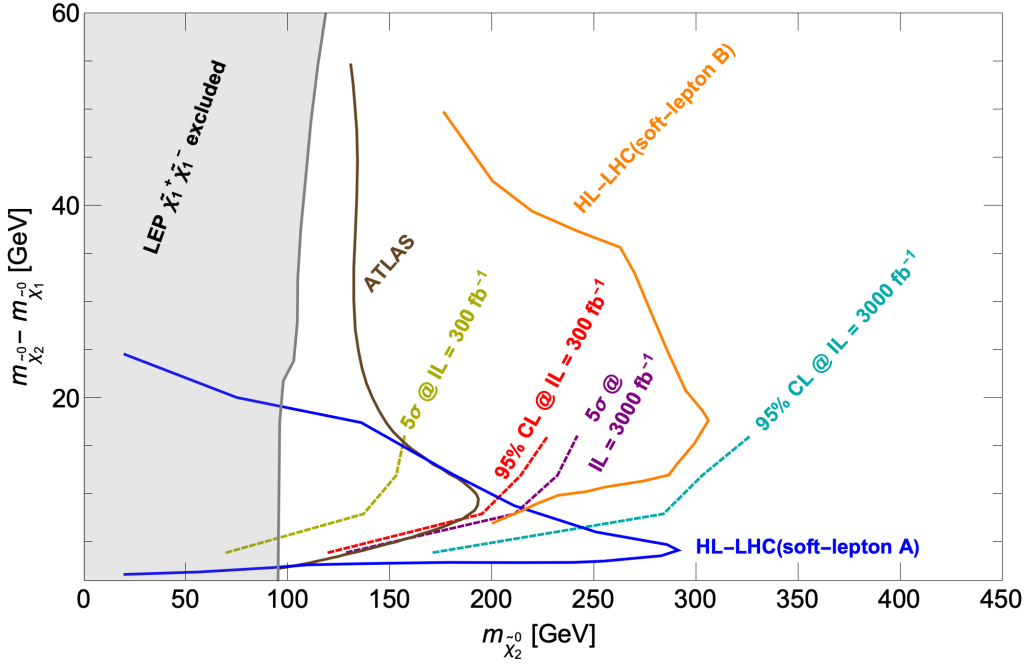


Figure 6: The projected 5σ reach and 95% CL exclusion contours for LHC14 with 300 and 3000 fb^{-1} in the $m_{\tilde{\chi}_2^0}$ vs. Δm plane after **C4** cuts. Also shown is the current 95% CL exclusion (ATLAS) and the projected 95% CL exclusions from two different analyses for the HL-LHC [26].

In Fig. 6, we translate the results of Fig. 5 into contours in the $m_{\tilde{\chi}_2^0}$ vs. Δm plane. The shaded region is excluded by LEP2 chargino searches. The region left of the contour labelled ATLAS is currently excluded by LHC searches at the 95%CL. We also show projections for what future searches at the HL-LHC would probe at the 95%CL [26]: ATLAS (soft-lepton A) and CMS (soft-lepton B). The various dashed contours show our projections for the signal reach. Our focus here has been on higgsino mass gaps $\lesssim 20 - 25$ GeV, that are generically expected in natural SUSY models. For larger mass gaps, it may be best to search for higgsinos via the hard multilepton events, without any requirement of a QCD jet. The reach projections in Fig. 6 may be compared to theoretical expectations, both from bottom-up naturalness considerations and from the string landscape [27].

Before closing this section, we note that we have only considered physics backgrounds in our analysis. The ATLAS collaboration [4] has, however, reported that a significant portion of the

background comes from fake leptons, both e and μ . Accounting for these detector-dependent backgrounds require data driven methods which are beyond the scope of our analysis. We remark, however, that for any specified value of the fake rate, it should be possible to make a rough estimate of the impact of the fakes on the reach contours in Fig. 6 using the cross sections in Fig. 5 since if the fakes increase the background by a factor f , the cross section necessary to maintain the same significance for the signal would have to increase by \sqrt{f} .

5 Summary

Light higgsinos of mass $\sim 100 - 400$ GeV with a compressed spectrum are the most robust prediction of natural supersymmetry, and could be the only directly accessible superpartners at the LHC. Here, we have re-examined the prospects for a search for soft opposite-sign/same flavor dilepton plus \cancel{E}_T from higgsino pair production in association with a hard monojet at the LHC. The dileptons originating from $\tilde{\chi}_2^0 \rightarrow \ell\bar{\ell}\tilde{\chi}_1^0$ would exhibit a distinctive kinematic edge with $m(\ell\bar{\ell}) < m_{\tilde{\chi}_2^0} - m_{\tilde{\chi}_1^0}$, while the monojet and the accompanying \cancel{E}_T serve as event triggers.

Our emphasis has been on the reduction of the main irreducible background to the higgsino signal from $\tau\bar{\tau}j$ production in the SM, where the soft leptons come from the decays of the taus. To this end, we have proposed angular cuts (see Sec. 3.1.2) which appear to be more efficient in reducing this background than the $m_{\tau\tau}^2$ cut that has been used by the ATLAS and CMS collaborations in their analysis of the higgsino signal. Of course, additional cuts are needed to further reduce the reducible background from $t\bar{t}$ production, and subdominant backgrounds from WWj , $W\ell\bar{\ell}j$ and $Z\ell\bar{\ell}j$ production. Table 2 shows a comparison between the new angular cuts and the currently used di-tau mass cut, and also provides a cut flow after various other analysis cuts discussed in the text.

Our final result is summarized by the dashed contours in Fig. 6. Our analysis works best for Δm values $\sim 15 - 20$ GeV but drops off for smaller and much larger mass gaps. We mention that mass gaps smaller than about 4 GeV occur only for very heavy gauginos that fail to satisfy naturalness expectations, while higgsinos with an increasingly uncompressed spectrum can be more effectively searched for via multilepton channels. We see from Fig. 6 that the HL-LHC with 3000 fb^{-1} gives a 5σ discovery reach to $m_{\tilde{\chi}_2^0} \sim 240$ GeV, with the 95% CL exclusion limit extending to ~ 325 GeV for $\Delta m \sim 16$ GeV. The signal reach would be even further enhanced if it becomes possible to extend the lepton acceptance to lower p_T values, or reliably increase b -quark rejection even beyond 80-85% that has already been achieved.

Acknowledgements:

This research is based upon work supported in part by the U.S. Department of Energy, Office of Science, Office of Basic Energy Sciences Energy Frontier Research Centers program under Award Number DE-SC-0009956 and U.S. Department of Energy Grant DE-SC-0017647. The work of DS was supported by the Ministry of Science and Technology (MOST) of Taiwan under Grant No. 110-2811-M-002-574.

References

- [1] K.L. Chan, U. Chattopadhyay and P. Nath, Phys. Rev. D **58** (1998) 096004; J. Feng, K. Matchev and T. Moroi, Phys. Rev. D **61** (2000) 075005; J. Feng K. Matchev and F. Wilczek, Phys. Lett. B **482** (2000) 388; R. Kitano and Y. Nomura, Phys. Lett, B **632** (2006) 162 and Phys. Rev. D **73** (2006) 095004; H. Baer, V. Barger and P. Huang, JHEP **11** (2011) 031; C. Brust, A. Katz, S. Lawrence and R. Sundrum, JHEP **03** (2012) 103; M. Papucci, J. Ruderman and A. Weiler, JHEP **09** (2012) 035; H. Baer, V. Barger, P. Huang and X. Tata, JHEP **05** (2012) 109.
- [2] H. Baer, V. Barger, P. Huang, A. Mustafayev and X. Tata, Phys. Rev. Lett. **109** (2012) 161802; H. Baer, V. Barger, P. Huang, D. Mickelson, A. Mustafayev and X. Tata, Phys. Rev. D **87** (2012) 115028.
- [3] H. Baer, V. Barger, H. Serce and X. Tata, Phys. Rev. D **94** (2016) 115017; H. Baer, V. Barger, M. Savoy, H. Serce and X. Tata, JHEP, **1706** (2017) 101.
- [4] G. Aad *et al.* [ATLAS Collaboration], Phys. Rev D **101** (2020) 052005, and references therein.
- [5] A. Tumasyan *et al.* [CMS Collaboration], arXiv:2111.06296 (2021), and references therein.
- [6] See H. Baer, V. Barger and P. Huang, Ref. [1].
- [7] H. Baer, A. Mustafayev and X. Tata, Phys. Rev. D **89** (2014) 055007; C. Han *et al.* JHEP **02** (2014) 049; P. Schwaller and J. Zurita, JHEP **03** (2014) 060.
- [8] H. Baer, A. Mustafayev and X. Tata, Ref. [7].
- [9] L. Carpenter, A. Nelson, C. Shimmin, T. Tait and D. Whiteson, Phys. Rev. D **87** (2013) 074005.
- [10] L. Carpenter, A. DiFranzo, M. Mulhearn, C. Shimmin and S. Tulin, Phys. Rev. D **89** (2017) 075017.
- [11] G. Giudice, T. Han, K. Wang and L-T. Wang, Phys. Rev. D **81** (2010) 115011.
- [12] Z. Han, G. D. Kribs, A. Martin and A. Menon, Phys. Rev. D **89** 075007 (2014);
- [13] H. Baer, A. Mustafayev and X. Tata, Phys. Rev. D **90** 115007 (2014).
- [14] C. Han, D. Kim, S. Munir and M. Park, JHEP **04** (2015) 132.
- [15] H. Baer, V. Barger, D. Sengupta and X. Tata, arXiv:2109.14030.
- [16] J. Alwall, M. Herquet, F. Maltoni, O. Mattelaer and T. Stelzer, JHEP **bf06**, 128 (2011).
- [17] T. Sjostrand, S. Mrenna and P. Z. Skands, JHEP **05**, 026 (2006).
- [18] J. de Favereau *et al.* [DELPHES 3], JHEP **02**, 057 (2014).

- [19] M. Cacciari, G. P. Salam and G. Soyez, JHEP **04**, 063 (2008).
- [20] M. Cacciari, G. P. Salam and G. Soyez, Eur. Phys. J. C **72**, 1896 (2012).
- [21] ATLAS collaboration, ATL-PHYS-PUB-2015-022.
- [22] F. E. Paige, S. D. Protopopescu, H. Baer and X. Tata, arXiv:hep-ph/0312045 [hep-ph].
- [23] H. Baer, V. Barger, H. Serce and X. Tata, Phys. Rev. D **94**, 115017 (2016).
- [24] M. Aaboud *et al.* [ATLAS], Phys. Rev. D **97** (2018) 052010.
- [25] R. Kadala, Ph. D. dissertation, arXiv:1205.1267; R. Kitano and Y. Nomura, Phys. Rev. D **73**, 095004 (2006).
- [26] A. Canepa, T. Han and X. Wang, Ann. Rev. Nucl. Part. Sci. **70** (2020) 425.
- [27] H. Baer, V. Barger, S. Salam, D. Sengupta and X. Tata, Phys. Lett. B **810**, 135777 (2020).